

ON THE ORBIT OF EXOPLANET WASP-12B

CHRISTOPHER J. CAMPO¹, JOSEPH HARRINGTON¹, RYAN A. HARDY¹, KEVIN B. STEVENSON¹, SARAH NYMEYER¹, DARIN RAGOZZINE², NATE B. LUST¹, DAVID R. ANDERSON³, ANDREW COLLIER-CAMERON⁴, JASMINA BLECIC¹, CHRISTOPHER B. T. BRITT¹, WILLIAM C. BOWMAN¹, PETER J. WHEATLEY⁵, THOMAS J. LOREDO⁶, DRAKE DEMING⁷, LESLIE HEBB⁸, COEL HELLIER³, PIERRE F. L. MAXTED³, DON POLLACO⁹, AND RICHARD G. WEST¹⁰

¹Planetary Sciences Group, Department of Physics, University of Central Florida, Orlando, FL 32816-2385, USA

²Harvard-Smithsonian Center for Astrophysics, 60 Garden St., Cambridge, MA 02138, USA

³Astrophysics Group, Keele University, Staffordshire ST5 5BG, UK

⁴School of Physics and Astronomy, University of St. Andrews, North Haugh, Fife KY16 9SS, UK

⁵Department of Physics, University of Warwick, Coventry, CV4 7AL, UK

⁶Department of Astronomy, Cornell University, Ithaca, NY 14853-6801, USA

⁷NASA's Goddard Space Flight Center, Greenbelt, MD 20771-0001, USA

⁸Department of Physics and Astronomy, Vanderbilt University, Nashville, TN 37235, USA

⁹Astrophysics Research Centre, School of Mathematics & Physics, Queen's University, University Road, Belfast, BT7 1NN, UK and

¹⁰Department of Physics and Astronomy, University of Leicester, Leicester, LE1 7RH, UK

(Received 2010 Mar 13; Accepted 2010 Oct 06)

ApJ, *in press*.

ABSTRACT

We observed two secondary eclipses of the exoplanet WASP-12b using the Infrared Array Camera on the *Spitzer Space Telescope*. The close proximity of WASP-12b to its G-type star results in extreme tidal forces capable of inducing apsidal precession with a period as short as a few decades. This precession would be measurable if the orbit had a significant eccentricity, leading to an estimate of the tidal Love number and an assessment of the degree of central concentration in the planetary interior. An initial ground-based secondary eclipse phase reported by López-Morales et al. (0.510 ± 0.002) implied eccentricity at the 4.5σ level. The spectroscopic orbit of Hebb et al. has eccentricity 0.049 ± 0.015 , a 3σ result, implying an eclipse phase of 0.509 ± 0.007 . However, there is a well documented tendency of spectroscopic data to overestimate small eccentricities. Our eclipse phases are 0.5010 ± 0.0006 (3.6 and 5.8 μm) and 0.5006 ± 0.0007 (4.5 and 8.0 μm). An unlikely orbital precession scenario invoking an alignment of the orbit during the *Spitzer* observations could have explained this apparent discrepancy, but the final eclipse phase of López-Morales et al. ($0.510 \pm^{+0.007}_{-0.006}$) is consistent with a circular orbit at better than 2σ . An orbit fit to all the available transit, eclipse, and radial-velocity data indicates precession at $< 1\sigma$; a non-precessing solution fits better. We also comment on analysis and reporting for *Spitzer* exoplanet data in light of recent re-analyses.

Subject headings: planetary systems — stars: individual: WASP-12 — techniques: photometric

1. INTRODUCTION

When exoplanets transit (pass in front of) their parent stars as viewed from Earth, one can constrain their sizes, masses, and orbits (Charbonneau et al. 2007; Winn 2009). Most transiting planets also pass behind their stars (secondary eclipse). This allows atmospheric characterization by measurement of planetary flux and constrains orbital eccentricity, e , through timing and duration of the eclipse (Kallrath & Milone 1999).

WASP-12b is one of the hottest transiting exoplanets discovered to date, with an equilibrium temperature of 2516 K for zero albedo and uniform redistribution of incident flux (Hebb et al. 2009). It also has a 1.09-day period, making it one of the shortest-period transiting planets. The close proximity to its host star (0.0229 ± 0.0008 AU, Hebb et al. 2009) should induce large tidal bulges on the planet's surface. Tidal evolution should quickly circularize such close-in orbits (Mardling 2007). Hebb et al. (2009) calculate a circularization time for WASP-12b as short as 3 Myr, much shorter than the estimated 2 Gyr age of WASP-12 or even the circularization times estimated for other hot Jupiters, given similar planetary tidal dissipation, though this calculation was based on a formalism

(Goldreich & Soter 1966) that ignores the influence of stellar tides and the coupling of eccentricity and semi-major axis in the evolution of the system. The influence of stellar tides could prolong the dissipation timescale to well over the age of the system (Jackson et al. 2008). The non-Keplerian gravitational potential may cause apsidal precession, measurable as secondary eclipse and transit timing variations over short time scales. WASP-12b also has an abnormally large radius ($R_p = 1.79 \pm 0.09$ Jupiter radii, R_J , Hebb et al. 2009) compared to those predicted by theoretical models (Bodenheimer et al. 2003; Fortney et al. 2007) and to other short-period planets. Tidal heating models assume non-zero e , and the heating rate can differ substantially for different values of e . WASP-12b's inflated radius may result from tidal heating, but this is difficult to justify if the orbit is circular (Li et al. 2010).

Ground-based observations by López-Morales et al. (2009) detected a secondary-eclipse phase for WASP-12b of 0.510 ± 0.002 , implying an eccentric orbit at the 4.5σ level (López-Morales et al. 2010 revised the uncertainty to $^{+0.007}_{-0.006}$). Radial velocity data (Hebb et al. 2009) find $e = 0.049 \pm 0.015$, a 3σ eccentricity, and predict an eclipse phase of 0.509 ± 0.007 . Given an eccentric orbit and the fast predicted precession time scale, WASP-12b makes an excellent candidate for the first

direct detection of exoplanetary apsidal precession. Such precession has been detected many times for eclipsing binary stars (Kreiner *et al.* 2001).

Against an orbit established by transit timings, precession would be apparent in just two eclipses, if sufficiently separated in time. For eccentric orbits, the eclipse-transit interval can differ from the transit-eclipse interval, and for precessing orbits this difference varies sinusoidally over one precession period. If the difference is insignificant, it places an upper limit on $e \cos \omega$, where ω is the argument of periastris. In the case of WASP-12b, which is expected to precess at a rate of $0.05^\circ \text{ d}^{-1}$ (Ragozzine & Wolf 2009), if the orbit is observed when $\omega \sim \pm 90^\circ$ and the effect on the eclipse timing is maximized, and assuming a timing precision of 0.0007 days, then secondary eclipse observations situated five months apart could detect precession at the 3σ level (see Equation 8). We note that the method of Batygin *et al.* 2009, based on the work of Mardling 2007 and extended to the three-dimensional case by Mardling 2010, is an indirect assessment of apsidal precession, since no orbital motion is actually observed. The technique, which only applies to multi-planet systems with a tidally affected inner planet and a nearby, eccentric, outer planet, cannot currently be applied to WASP-12b.

Paired with the López-Morales *et al.* data, our *Spitzer Space Telescope* (Werner *et al.* 2004) eclipse observations provide a one-year baseline. *Spitzer's* high photometric precision also allows an accurate assessment of $e \cos \omega$. One can solve for e and ω separately given $e \sin \omega$ from precise radial velocity data. The following sections present our observations; photometric analysis; a dynamical model that considers parameters from this work, the original and revised parameters of López-Morales *et al.*, Hebb *et al.*, new transit times from the Wide-Angle Search for Planets (WASP), and transit times from a network of amateur astronomers; and our conclusions.

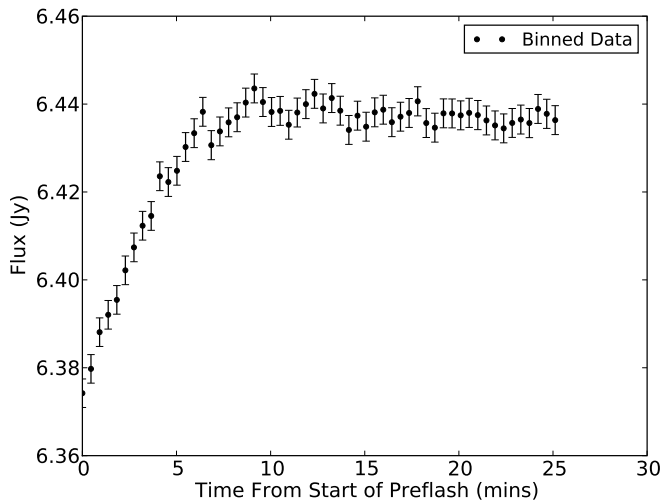


FIG. 1.— Preflash light curve. These are channel-4 ($8 \mu\text{m}$ data, analyzed with aperture photometry at the pixel location of the eclipse observations. The preflash source is bright compared to WASP-12, which allows the array sensitivity to “ramp” up before the science observations. Without a preflash, similar observations generally show a steeper and longer ramp in the eclipse observations.

2. OBSERVATIONS

We observed two secondary eclipses of WASP-12b with the *Spitzer* Infrared Array Camera (IRAC, Fazio *et al.* 2004) in full-array mode. Observations on 2008 October 29 at 4.5

and $8.0 \mu\text{m}$ (IRAC channels 2 and 4, respectively) lasted 338 minutes (program ID 50759); those on 2008 November 3 at 3.6 and $5.8 \mu\text{m}$ (channels 1 and 3, respectively) lasted 368 minutes (Program ID 50517). The IRAC beam splitter enabled simultaneous observations in the paired channels; all exposures were 12 seconds, resulting in 1696 frames in each of channels 1 and 3 and 1549 frames in each of channels 2 and 4. To minimize inter-pixel variability in all channels and the known intra-pixel variability in channels 1 and 2 (Reach *et al.* 2005; Charbonneau *et al.* 2005; Harrington *et al.* 2007; Stevenson *et al.* 2010), each target had fixed pointing. Prior to the science observations in channels 2 and 4, we observed a 57-frame preflash, exposing the array to a relatively bright source to reduce the time-dependent sensitivity (“ramp”) effect in channel 4 (Charbonneau *et al.* 2005; Harrington *et al.* 2007; Knutson *et al.* 2008, see Figure 1). Each observation ended with a 10-frame, post-eclipse observation of blank sky in the same array position as the science observations to check for warm pixels in the photometric aperture.

3. DATA ANALYSIS

Spitzer's data pipeline (version S18.7.0) applied both standard and IRAC-specific corrections, producing the Basic Calibrated Data (BCD) we analyzed. Our analysis pipeline masks pixels according to *Spitzer's* permanent bad pixel masks. It masks additional bad pixels (e.g., from cosmic-ray strikes), by grouping frames into sets of 64 and doing a two-iteration outlier rejection at each pixel location. Within each array position in each set, this routine calculates the standard deviation from the *median*, masks any pixels with greater than 4σ deviation, and repeats this procedure once. Masked pixels do not participate in the analysis.

The channel-4 data show a horizontal streak of pixels with low fluxes located ~ 10 pixels above the star. A similar diagonal streak appears ~ 10 pixels below and left of the star. This artifact, which we masked, resulted from saturation in a prior observation. A two-dimensional Gaussian fit found the photometry center for each image (Stevenson *et al.* 2010, see the Supplementary Information for discussion of centering methods on *Spitzer* data). The pipeline uses interpolated aperture photometry (Harrington *et al.* 2007), ignoring frames with masked pixels in the photometry aperture and not using masked pixels in sky level averages. Table 1 presents photometry parameters. We evaluated numerous photometry apertures (see Table 5 in the appendix), choosing the one with the best final light-curve fit in each channel (see below). Because channel 4 had a higher background flux level, the best sky annulus was larger and the photometry aperture was smaller than in the other channels. The channel-4 aperture contained 63% of the point-spread function; the others contained 89% or more.

The intra-pixel variation only affects channels 1 and 2, and was only substantial in channel 1 (see Table 1 and Figure 2). We model the intra-pixel effect with a second-order, two-dimensional polynomial,

$$V_{IP}(x, y) = p_1 y^2 + p_2 x^2 + p_3 xy + p_4 y + p_5 x + 1, \quad (1)$$

where x and y are the centroid coordinates relative to the pixel center nearest the median position and p_1 , p_2 , p_3 , p_4 , and p_5 can be free parameters. We model the ramp for channel 1 with the rising exponential

$$R(t) = 1 - \exp(-r_1[t - r_2]), \quad (2)$$

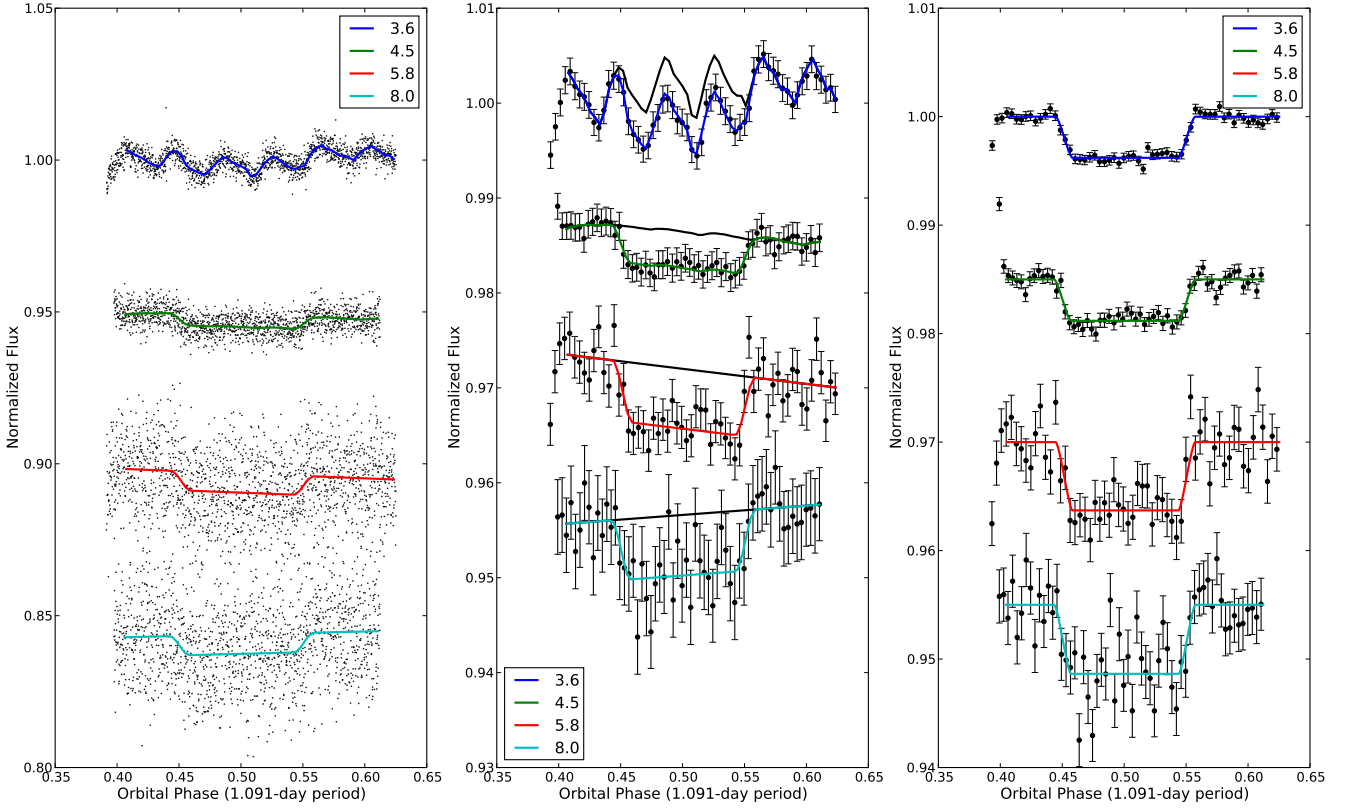


FIG. 2.— Raw (left), binned (center), and systematics-corrected (right) secondary eclipse light curves of WASP-12b in the four IRAC channels, normalized to the mean system flux within the fitted data. Colored lines are the best-fit models; black curves omit their eclipse model elements. A few initial points in all channels are not fit, as indicated, to allow the telescope pointing and instrument to stabilize.

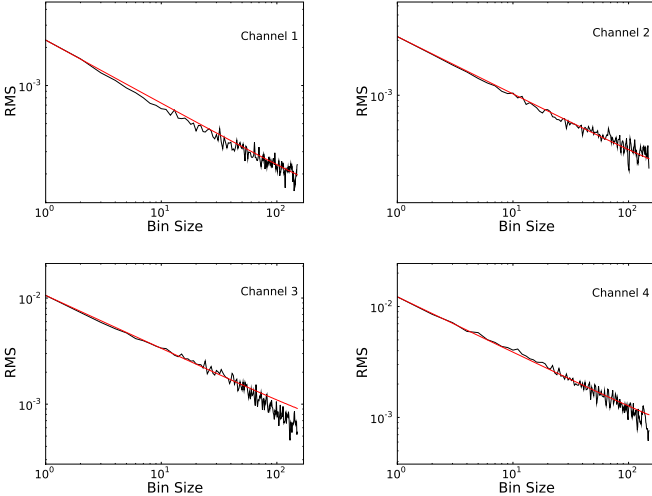


FIG. 3.— Root-mean-squared (RMS) residual flux vs. bin size in each channel. This plot tests for correlated noise. The straight line is the prediction for Gaussian white noise. Since the data do not deviate far from the line, the effect of correlated noise is minimal.

where t is orbital phase and r_1 and r_2 are free parameters. The remaining channels used a linear model,

$$R(t) = r_3(t - 0.5) + 1, \quad (3)$$

where r_3 is a free parameter. The eclipse, $E(t)$, is a Mandel & Agol (2002) model, assuming no limb darkening. The final light-curve model is

$$F(x, y, t) = F_s V_{IP}(x, y) R(t) E(t), \quad (4)$$

where $F(x, y, t)$ is the flux measured from interpolated aperture photometry and F_s is the (constant) system flux outside of eclipse, including the planet.

To estimate photometric uncertainties, we propagate the values in the *Spitzer* BCD uncertainty images through the aperture photometry calculation. Since the *Spitzer* pipeline generally overestimates uncertainties, we fit an initial model with a χ^2 minimizer and then scale all uncertainties to give a reduced χ^2 of unity (Harrington et al. 2007). We confirm the fit by redoing it with the new uncertainties. The scaling factor is proportional to the standard deviation of the normalized residuals (SDNR) from the models, as reported in Tables 5 (in the appendix) and 1. The $\sim 2\%$ SDNR variation does not significantly affect the fits. To select among models, we must compare fits made to the same data, including uncertainties. So, we use just one uncertainty scaling factor for all models in each combination of aperture and channel (see Tables 1 and 5 in the appendix).

Sivia & Skilling (2006) provide an accessible tutorial to the Bayesian approach of our subsequent analysis. MacKay (2003, chapter 29, and especially section 4) introduces Markov-Chain Monte Carlo (MCMC) and discusses its practicalities. Briefly, the MCMC algorithm calculates χ^2 at random locations near the χ^2 minimum in the parameter phase space, accepting only some of these steps for later analysis. The density of these accepted points is proportional to the probability of a model at that location, given the data. The attraction of MCMC is that histograms and scatter plots of subsets of interesting parameters from the accepted points display parameter uncertainties and correlations in a way that fully accounts for the uncertainties in and correlations with

TABLE 1
 JOINT LIGHT-CURVE FIT PARAMETERS

Parameter	3.6 μm	4.5 μm	5.7 μm	8.0 μm
Array Position (\bar{x} , pix)	25.20	20.24	19.35	21.45
Array Position (\bar{y} , pix)	26.98	27.95	27.15	25.67
Position Consistency ^a (δ_x , pix)	0.012	0.013	0.030	0.13
Position Consistency ^a (δ_y , pix)	0.012	0.013	0.018	0.14
Aperture Size (pix)	3.75	4.00	2.75	2.00
Sky Annulus Inner Radius (pix)	7.00	7.00	7.00	12.00
Sky Annulus Outer Radius (pix)	12.00	12.00	12.00	30.00
System Flux F_s (μJy)	25922 \pm 11	16614 \pm 3	11129 \pm 4	6111 \pm 3
Eclipse Depth ^c (F_p/F_*)	0.00379 \pm 0.00013	0.00382 \pm 0.00019	0.00629 \pm 0.00052	0.00636 \pm 0.00067
Brightness Temperature (K)	2740 \pm 49	2571 \pm 73	3073 \pm 176	2948 \pm 233
Eclipse Mid-time ^{b, c} (t_{mid} , phase)	0.5010 \pm 0.0006	0.5006 \pm 0.0007	0.5010 \pm 0.0006	0.5006 \pm 0.0007
Eclipse Mid-time ^d (t_{mid} , BJD - 2,454,000)	773.6481 \pm 0.0006	769.2819 \pm 0.0008	773.6481 \pm 0.0006	769.2819 \pm 0.0008
Eclipse Duration ^c (t_{4-1} , sec)	10615.66 \pm 102.95	10749.97 \pm 142.72	10615.66 \pm 102.95	10749.97 \pm 142.72
Ingress Time (t_{2-1} , sec)	1266.43	1266.43	1266.43	1266.43
Egress Time (t_{4-3} , sec)	1266.43	1266.43	1266.43	1266.43
Ramp Name	Rising Exponential	Linear	Linear	Linear
Ramp, Curvature ^c (r_1)	29 \pm 1	0	0	0
Ramp, Phase Offset ^c (r_2)	0.17747	0.5	0.5	0.5
Ramp, Linear Term ^c (r_3)	0	-0.0102 \pm 0.0015	-0.016 \pm 0.004	0.010 \pm 0.005
Intra-pixel, Quadratic Term in y^c (p_1)	0	-0.09 \pm 0.04	0	0
Intra-pixel, Quadratic Term in x^c (p_2)	-0.140 \pm 0.011	0	0	0
Intra-pixel, Cross Term (p_3)	0	0	0	0
Intra-pixel, Linear Term in y^c (p_4)	0.086 \pm 0.004	0	0	0
Intra-pixel, Linear Term in x (p_5)	0	0	0	0
Total frames	1697	1560	1697	1560
Good frames ^e	1532	1457	1543	1467
Rejected frames ^e (%)	9	6	9	5
Free Parameters	10	9	10	9
Number of Data Points in Fit	3075	2924	3075	2924
BIC	3155.5	2996.0	3155.5	2996.0
AIC	3095.7	2942.2	3095.7	2942.2
Standard Deviation of Normalized Residuals	0.00228716	0.00324027	0.01058880	0.01222100
Uncertainty Scaling Factor	0.31248	0.44500	0.91832	0.62475

^a RMS frame-to-frame position difference.

^b Based on the transit ephemeris time given by Hebb *et al.* (2009).

^c MCMC jump parameter.

^d Uncorrected for light-travel time in the exoplanetary system (see Dynamics section).

^e We reject frames during instrument/telescope settling and with bad pixels in the photometry aperture.

the uninteresting parameters. These are called marginal distributions.

We fit equation 4 with a χ^2 minimizer and assess parameter uncertainties with a Metropolis random-walk (MRW) MCMC algorithm. Our MRW used independent Gaussian proposal distributions for each parameter with widths chosen to give an acceptance rate of 20 – 60% of the steps. See Figures 6 and 7 for marginal distributions for the final models.

The intent of MCMC is to explore the phase space, not to find one optimal model. Even the best model in an MCMC chain is not a good replacement for the model found by a minimizer, because MCMC is unlikely to land *exactly* on the minimum that a minimizer easily finds to machine precision. If an MCMC chain finds a lower χ^2 value than the minimizer's, then it has entered the basin of attraction around a better local minimum, and a minimizer will almost certainly find an even better χ^2 starting from the MCMC's best value. We thus refit at such points and then restart our MCMC routine from the new minimizer solution. The χ^2 used in the information criteria described below refers to the global minimum of a given dataset and not merely the sampled minimum from MCMC. Although the differences may appear to be small, at the extreme precisions required for high-contrast photometry and models with many parameters, parameter values can differ by a significant fraction of 1σ between the global and MCMC minima, even for converged chains.

The MCMC routine ran an initial “burn in” of a least 10^5 iterations to forget the initial starting conditions, and then used two million iterations to sample the phase space near the fit solution. To test for adequate sampling, we ran four independent MCMC chains, three started away from the initial minimizer location, and calculated the Gelman & Rubin (1992) statistic for each parameter. These were all within 1% of unity, indicating the chains converged. We initially fit each channel separately with all free model parameters as MCMC jump parameters (see Table 5 in the appendix). Then we pair the channels observed together, fitting a common eclipse phase and duration (see Table 1). Due to high correlations, the MCMC sampling becomes very inefficient with all the parameters free in the joint fit. Estimates of the interesting parameters (eclipse depth, time, and duration) are unaffected if we freeze r_2 and the ingress and egress times at several different values. We set r_2 from the independent light-curve fits and the ingress and egress times as predicted by the (Hebb *et al.* 2009) orbit.

A recent re-analysis of older data by Knutson *et al.* (2009) demonstrates that the complex models required to fit *Spitzer's* systematics can have multiple, comparable χ^2 minima in different parts of phase space. These minima may change their relative depths given different systematic models (e.g., exponential vs. log-plus-linear ramps), resulting in different conclusions. To control for this, we fit data from a range of photometry apertures with many combinations of analytic model

components (see Table 5 in the appendix) before choosing Eq. 1 – Eq. 3. The models included quadratic and logarithmic-plus-linear ramps and a variety of polynomial intrapixel models. Additionally, we drop a small number of initial points to allow the pointing and instrument to stabilize, which vastly improved the fits.

Choices among photometry apertures and numbers of dropped points are choices between different datasets fit with the same models, so we minimize the SDNR, removing the fewest points consistent with low SDNR. The model lines in Figure 2 show the included points.

Once we have selected the dataset (by choice of aperture and dropped points according to SDNR), we may apply any of several information criteria to compare models with different numbers of free parameters (Liddle 2007). These criteria have specific goals and assumptions, so none is perfectly general, but two have broad application. The Akaike Information Criterion,

$$\text{AIC} = \chi^2 + 2k, \quad (5)$$

where k is the number of free parameters, applies when the goal is accurate prediction of future data; its derivation is valid even when the candidate models might not include the theoretically correct one (as is the case, so far, for *Spitzer* intrapixel and ramp modeling). The Bayesian Information Criterion,

$$\text{BIC} = \chi^2 + k \ln N, \quad (6)$$

where N is the number of data points, applies when the goal is identifying the theoretically correct model, which is known to be one of those being considered. The best model minimizes the chosen information criterion. The ratio of probabilities favoring one model over another is $\exp(\Delta\text{BIC}/2)$, where ΔBIC is the difference in BIC between models, but the difference in AIC between models has no simple calibration to a probability or significance level.

These goals give different answers for finite datasets. If the right model is a candidate, the BIC will do better than AIC as the number of points increases; if not, which is better depends on the sample size and on how close the candidate models are to the (absent) correct model. Other information criteria exist, but are either tailored to specific circumstances or are still being vetted by statisticians. The criteria solve different problems, but the goal of a multi-model analysis is not always easily classified as solely predictive or explanatory, so there is some elasticity regarding the choice of an appropriate criterion.

We calculate AIC and BIC for hundreds of models, and reject most of them on this basis (see Table 5 in the appendix). For the final decision, we also consider the level of correlation in the residuals. For this, we plot root-mean-squared (RMS) model residuals *vs.* bin size (Pont et al. 2006, Winn et al. 2008) and compare to the theoretical $1/\sqrt{N}$ RMS scaling. Figure 3 demonstrates the lack of significant photometric noise correlation in our final models. In some cases, we prefer less-correlated models with insignificantly poorer AIC or BIC (e.g., channel 1). Differences in interesting parameter values (eclipse depth, time, and duration) for such near-optimal alternatives are $\lesssim 1\sigma$.

Given the questions raised by re-analyses of certain *Spitzer* exoplanet datasets (Knutson et al. 2009; Beaulieu et al. 2010), we consider it critical that investigators disclose the details of their analyses both so that readers can assess the quality of the analysis and so that others may make meaningful compar-

isons in subsequent analyses of the same data (e.g., did they find a better χ^2 ?). It is important to include a full description of the centering, photometry, uncertainty assessment, model fitting, correlation tests, phase-space exploration, and convergence tests. A listing of alternative model fits and their quality may build confidence that there is not a much better model than those tried. One must identify the particular χ^2 minimum explored by reporting even nuisance parameter values, such as those in the intrapixel and ramp curves.

Finally, the marginal posterior distributions (i.e., the parameter histograms) and plots of their pairwise correlations help in assessing whether the phase space minimum is global and in determining parameter uncertainties. We present these plots for the astrophysical parameters in Figures 4, 5, 6, & 7. The electronic supplement to this article includes data files containing the photometry, best-fit models, centering data, etc.. We encourage all investigators to make similar disclosure in future reports of exoplanetary transits and eclipses.

4. DYNAMICS

Hebb et al. (2009) detect a non-zero eccentricity for WASP-12b that should be observable in the timing of the secondary eclipse. Our two secondary eclipse phases (Table 1) are within 2σ of $\phi = 0.5$ for the Hebb et al. (2009) ephemeris, and taken together imply $e \cos \omega = 0.0016 \pm 0.0007$. This indicates that if the planet’s orbit is eccentric, then ω is closely aligned with our line of sight. Recognizing the unlikelihood of this configuration (which implicitly questions the López-Morales et al. 2009 eclipse phase), this section nonetheless considers the possibility of significant eccentricity, with precession between the López-Morales et al. (2009) eclipse phase and *Spitzer*’s. Subsequent to the initial submission of this paper, López-Morales et al. (2010) increased their uncertainty by a factor of three. Since the arXiv postings of both López-Morales et al. (2009) and the submitted version of this paper (arXiv 1003.2763v1) raised some community discussion, we now treat both cases to explain how this adjustment changes our conclusions.

We use an MCMC routine to fit a Keplerian model of the planet’s orbit to our secondary eclipse times, radial velocity data (Hebb et al. 2009), transit timing data provided by the WASP team and amateur observers (Table 2), and the ground-based secondary eclipse measurement of López-Morales et al. (2009, 2010). Because López-Morales et al. folded 1.5 complete eclipses, we represent their point as a single observation taken during an orbit halfway between their eclipses (HJD 2455002.8560 \pm 0.0024). We remove three in-transit radial velocity points due to Rossiter-McLaughlin contamination, and correct the times of mid-eclipse given in Table 1 and by López-Morales et al. (2009, 2010) for light travel across the orbit by subtracting 22.8 seconds. We note that eclipse observers should report uncorrected times, as the correction depends on the orbit model and, in the future, measurements may be uncertain at the level of model uncertainty.

The amateur observers synchronize their clocks to within one second of UTC by means such as Network Time Protocol (NTP) or radio signals from atomic clocks. In pre-publication discussions with Eastman et al. (2010), we determined that the amateurs’ observing software, MaximDL, did not account for leap seconds, nor did the software of most of our professional contributors. We thus made the adjustment ourselves as needed.

TABLE 2
TRANSIT TIMING DATA

Mid-Transit Time (HJD)	Uncertainty	Source ^a
2453264.7594	0.0048	WASP Team
2454120.4290	0.0070	WASP Team
2454129.1600	0.0017	WASP Team
2454508.9761	0.0002	Hebb et al. (2009)
2454515.52464	0.00016	WASP Team
2454552.6218	0.0034	WASP Team
2454836.4026	0.0006	Veli-Pekka Hentunen, AXA
2454837.4955	0.0013	Alessandro Marchini, AXA
2454840.7704	0.001	Bruce Gary, AXA
2454848.41003	0.00213	František Lomoz, TRESCA
2454860.41473	0.0023	Yenal Ögmen, TRESCA
2454860.4176	0.00132	Jaroslav Trnka, TRESCA
2454883.33312	0.0056	Alessandro Marchini, AXA
2454908.4372	0.001	Ramon Naves, AXA
2454931.35739	0.00098	Lubos Brát, TRESCA
2455136.54322	0.00066	Leonard Kornos and Peter Veres, TRESCA
2455151.82129	0.00141	Stan Shadick, TRESCA
2455164.92317	0.00149	Stan Shadick, TRESCA
2455172.5620	0.00014	Mikael Ingemyr, TRESCA
2455197.6628	0.00203	Brian Tieman, TRESCA
2455198.75595	0.00141	Brian Tieman, TRESCA
2455219.48996	0.00131	Lubos Brát, TRESCA

^a The Amateur Exoplanet Archive (AXA, <http://brucegary.net/AXA/x.htm>) and Transiting ExoplanetS and Candidates group (TRESCA, <http://var2.astro.cz/EN/tresca/index.php>) supply their data to the Exoplanet Transit Database (ETD, <http://var2.astro.cz/ETD/>), which performs the uniform transit analysis described by Poddaný et al. (2010). The ETD web site provided the AXA and TRESCA numbers in this table.

TABLE 3
ORBITAL FITS

Parameter	No Precession	With Precession
$e \sin \omega_0^a$	-0.065 ± 0.014	-0.065 ± 0.014
$e \cos \omega_0^a$	0.0014 ± 0.0007	-0.0058 ± 0.0027
e	0.065 ± 0.014	0.065 ± 0.014
ω_0 (°)	-88.8 ± 0.9	-95.1 ± 2.3
$\dot{\omega}$ (° d ⁻¹) ^a	0 ± 0	0.026 ± 0.009
P_s (days) ^a	$1.0914240 \pm 3 \times 10^{-7}$	$1.091436 \pm 4 \times 10^{-6}$
P_a (days)	$1.0914240 \pm 3 \times 10^{-7}$	$1.091521 \pm 3 \times 10^{-5}$
T_0 (MJD) ^{a,b}	508.97686 ± 0.00012	508.97686 ± 0.00012
K (ms ⁻¹) ^a	224 ± 4	224 ± 4
γ (ms ⁻¹) ^a	19087 ± 3	19088 ± 3
BIC	101.0	97.6

^a MCMC Jump Parameter.

^b MJD = JD - 2,454,000.

In our model,

$$\chi^2 = \sum \left(\frac{v_{rv,o} - v_{rv,m}}{\sigma_{rv}} \right)^2 + \sum \left(\frac{t_{tr,o} - t_{tr,m}}{\sigma_{tr}} \right)^2 + \sum \left(\frac{t_{ecl,o} - t_{ecl,m}}{\sigma_{ecl}} \right)^2, \quad (7)$$

where $v_{rv,o}$, $t_{tr,o}$, $t_{ecl,o}$ are the observed radial velocities, transit times, and eclipse times, respectively; σ_{rv} , σ_{tr} , σ_{ecl} are their respective uncertainties, and $v_{rv,m}$, $t_{tr,m}$, $t_{ecl,m}$ are the respective model calculations.

Table 3 gives our best-fit results using the original López-Morales et al. (2009); differences from our arXiv posting are due to the time corrections and the use of a minimizer to find the true χ^2 minimum. The eccentricity of $e = 0.065 \pm 0.014$

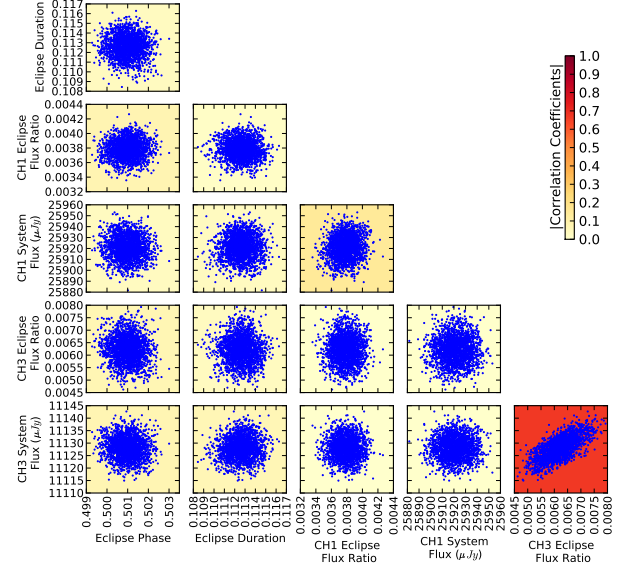


FIG. 4.— Parameter correlations for 3.6 and 5.8 μm . To decorrelate the Markov chains and unclutter the plot, one point appears for every 1000th MCMC step. Each panel contains all the points.

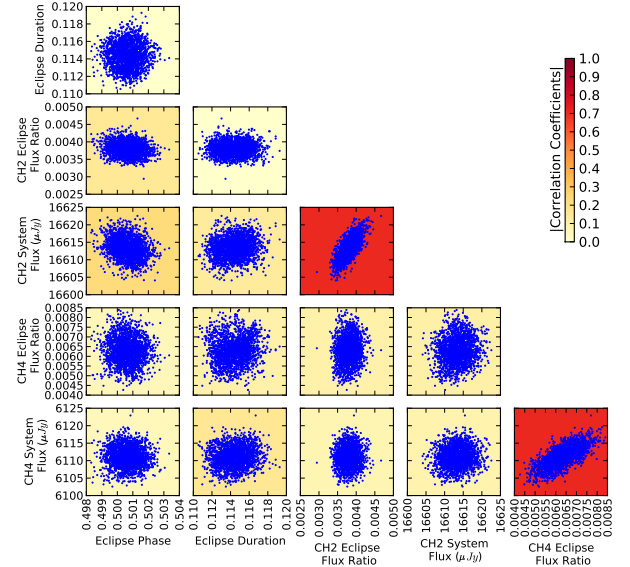


FIG. 5.— Parameter correlations for 4.5 and 8.0 μm . To decorrelate the Markov chains and unclutter the plot, one point appears for every 1000th MCMC step. Each panel contains all the points.

may be high due to poor constraints on $e \sin \omega$. Our dynamical fits considered only the transit and eclipse times and did not directly fit the light curves, which could additionally have modeled variable eclipse and transit durations.

A significantly positive eccentricity implies either extremely low tidal dissipation (e.g., $Q_p \gtrsim 10^8$; a tidal evolution model could give a better limit, Mardling 2007, Levrard et al. 2009) or a perturber such as another planet. In the latter case, coupling between the two planets could potentially drain energy and angular momentum from the outer orbit to the point where it is not able to maintain a large eccentricity for WASP-12b (e.g., Mardling 2007). Tidal dissipation of a

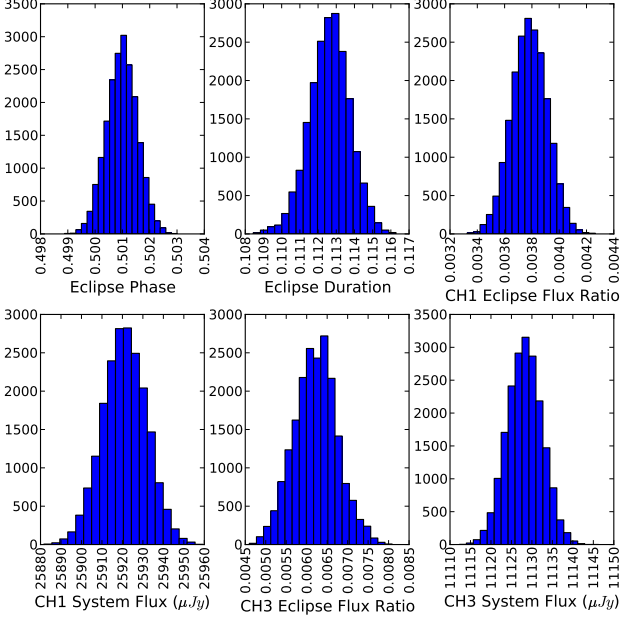


FIG. 6.— Parameter histograms for 3.6 and 5.8 μm . To decorrelate the Markov chains, the histograms come from every 100th MCMC step.

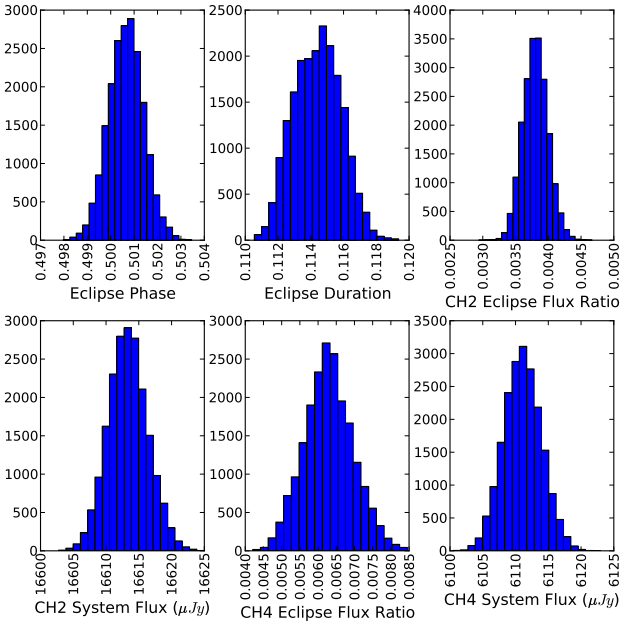


FIG. 7.— Parameter histograms for 4.5 and 8.0 μm . To decorrelate the Markov chains, the histograms come from every 100th MCMC step.

non-zero eccentricity could account for the inflated radius of WASP-12b. If the orbit is actually circular, the bloated size (Hebb et al. 2009) requires either an energy source or new interior models.

As noted above, the planet’s proximity to its star must raise huge tidal bulges (Ragozzine & Wolf 2009) that significantly contribute to an aspherical planetary gravitational potential. This would induce apsidal precession measurable over short timescales through transit and eclipse timing variations. The rate of precession is proportional to the tidal Love number,

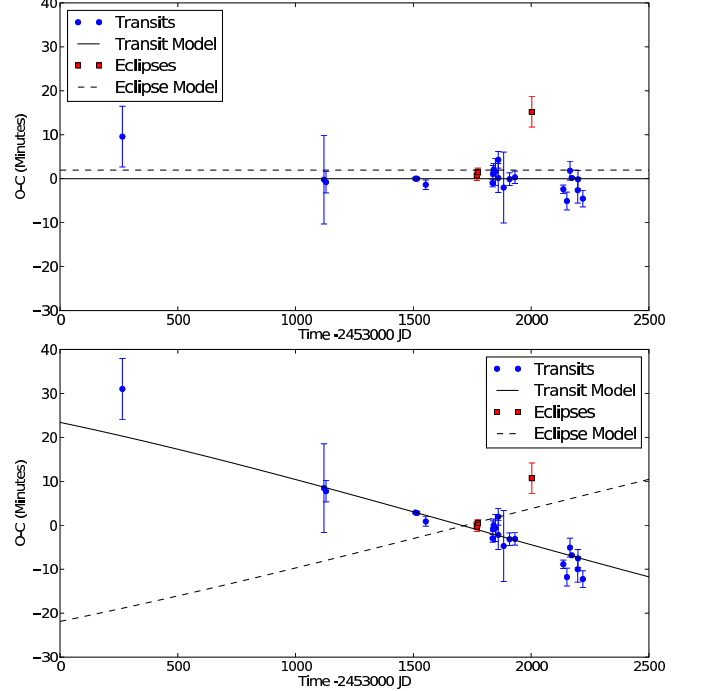


FIG. 8.— Transit times and orbit models of Table 3. Top: Non-precessing case. Bottom: Precessing case. Both diagrams show the difference (observed-minus-calculated, O-C) from a linear ephemeris determined from P_s and T_0 given for their respective cases in Table 3. This highlights deviations from the ephemeris. The dashed lines give eclipse times for the eccentric orbits of the fits. In the non-precessing case, these lines are straight and horizontal, and the transits (which carry the most weight in determining the period) scatter about the line, as expected. However, the López-Morales et al. (2009) point suggests a trend in the eclipses consistent with apsidal precession. In the precessing case, the models are opposing sinusoids with a ~ 32 -minute amplitude and a 33-year period. The curves cross approximately where $\omega = -90^\circ$. Both curves and data were shifted upward by $-\frac{eP_a}{\pi} \cos \omega_0$ (about 2 minutes) to adjust for the modification in Eq. 8, so the curves cross where O-C = 0.

k_{2p} , which describes the concentration of the planet’s interior mass (Ragozzine & Wolf 2009). A lower k_{2p} implies more central condensation, but k_{2p} alone does not define a unique density profile (Batygin et al. 2009). A nominal value of $k_{2p} = 0.3$ yields precession of $\sim 0.05^\circ \text{d}^{-1}$ for the orbit of WASP-12b. A precise measurement of the precession rate will therefore constrain the planet’s internal structure, as long as the eccentricity is significantly non-zero (Ragozzine & Wolf 2009). Conversely, the absence of observable precession limits the eccentricity.

We added a constant precession term, $\dot{\omega}$, to our model, and took the inclination to be $\sim 90^\circ$, as the timing effects due to inclination should be negligible and the available timing data cannot directly constrain this quantity. With these assumptions we modified Eq. 15 of Giménez & Bastero (1995) such that

$$T_{\text{tr}} = T_0 + P_s E - \frac{eP_a}{\pi} (\cos \omega_{\text{tr}} - \cos \omega_0), \quad (8)$$

where T_{tr} is the time of mid-transit, T_0 is the transit time at orbit zero, P_s is the sidereal period, and P_a is the anomalistic period, or time between successive periastron passages. The right bracket indicates truncation of a series. Furthermore, P_a

is related to P_s by

$$P_a = \frac{P_s}{1 - P_s \frac{\dot{\omega}}{2\pi}}. \quad (9)$$

E is the number of elapsed sidereal periods since T_0 and $\omega_{tr} = \dot{\omega}(T_{tr} - T_0) + \omega_0$, where ω_0 is ω at T_0 . We expand the equation to fifth order in e and solve iteratively for T_{tr} . We compute the eclipse time as a function of e , ω_{tr} , P_a , and T_{tr} ; radial velocity is computed as a function of $\omega(t)$.

Fitting this model to the data with the López-Morales *et al.* (2009) point, we found that $\dot{\omega} = 0.026 \pm 0.009^\circ \text{d}^{-1}$, a 3σ result. This corresponds to a precession period of 33 ± 13 years and implies that $k_{2p} = 0.15 \pm 0.08$ (see Table 3). This result depended on an unlikely alignment of the orbit with our line of sight during the *Spitzer* observations. The revised López-Morales *et al.* (2010) uncertainty dashed hopes for detecting precession, however, as the model fit with that point (Table 4) yields a marginal precession, and BIC prefers the non-precessing case. Even if the 4σ eccentricity stands, measurement of precession awaits a longer observational baseline.

5. CONCLUSIONS

The timing of the *Spitzer* eclipses is consistent with a circular orbit, and our best fit, including RV data and transit and eclipse times, does not detect precession.

Although the López-Morales *et al.* (2010) eclipse phase is now marginally consistent with zero eccentricity, we note that this $0.9\text{-}\mu\text{m}$ observation could be affected by a wavelength-dependent asymmetry in the planet’s surface-brightness distribution that manifests itself as a timing offset (Knutson *et al.* 2007). This offset has a maximum possible value of $R_p/v_p \approx 9$ minutes, where v_p is the planet’s orbital velocity. This is somewhat smaller than the observed variation in eclipse timing between López-Morales *et al.* (2010) and *Spitzer*.

While we have not yet measured precession, the possible prolateness should be measurable in high-accuracy, infrared transits and eclipses (Ragozzine & Wolf 2009), such as we expect will be available from the James Webb Space Telescope. This would provide another constraint on interior structure, one that does not depend on an elliptical orbit.

As this paper was in late stages of revision, Croll *et al.* (2010) published three ground-based secondary eclipses and Husnoo *et al.* (2010) produced additional radial velocity data. These datasets are consistent with a circular orbit for WASP-12b.

As the quality of these data attests (the signal-to-noise ratio

of the eclipse depth in channel 1 is over 29, second only to that for HD 189733b), WASP-12b has emerged as a highly observable exoplanet. Madhusudhan *et al.* (2010) report our analysis of the planet’s atmospheric composition. Its phase curves, already in *Spitzer*’s queue, will enable the first observational discussion of atmospheric dynamics on a prolate planet.

We thank the observers listed in Table 2 for allowing us to use their results, and the organizers of the Exoplanet Transit Database for coordinating the collection and uniform analysis of these data. The IRAC data are based on observations made with the *Spitzer* Space Telescope, which is operated by the Jet Propulsion Laboratory, California Institute of Technology under a contract with NASA. Support for this work was provided by NASA through an award issued by JPL/Caltech. The point

TABLE 4
REVISED ORBITAL FITS

Parameter	No Precession	With Precession
$e \sin \omega_0^a$	-0.063 ± 0.014	-0.065 ± 0.015
$e \cos \omega_0^a$	0.0011 ± 0.00072	-0.0036 ± 0.0045
e	0.063 ± 0.014	0.065 ± 0.015
ω_0 ($^\circ$)	-89.0 ± 0.8	-93 ± 5
$\dot{\omega}$ ($^\circ \text{d}^{-1a}$)	0 ± 0	0.017 ± 0.019
P_s (days) ^a	$1.0914240 \pm 3 \times 10^{-7}$	$1.0914315 \pm 7 \times 10^{-6}$
P_a (days)	$1.0914240 \pm 3 \times 10^{-7}$	$1.0914872 \pm 7 \times 10^{-5}$
T_0 (MJD) ^{a,b}	508.97683 ± 0.00012	508.97685 ± 0.00012
K (ms^{-1a})	225 ± 4	224 ± 4
γ (ms^{-1a})	19087 ± 3	19088 ± 3
BIC	90.1	92.8

^a MCMC Jump Parameter.

^b MJD = JD - 2,454,000.

of M. Ingemyr is based on observations made with the Nordic Optical Telescope (NOT), operated on the island of La Palma jointly by Denmark, Finland, Iceland, Norway, and Sweden, in the Spanish Observatorio del Roque de los Muchachos Instituto Astrofísica de Canarias, and ALFOSC, which is owned by the Instituto Astrofísica de Andalucía (IAA) and operated at the NOT under agreement between IAA and NBIfAFG of the Astronomical Observatory of Copenhagen. We thank contributors to SciPy, Matplotlib, and the Python Programming Language, W. Landsman and other contributors to the Interactive Data Language Astronomy Library, the free and open-source community, the NASA Astrophysics Data System, and the JPL Solar System Dynamics group for free software and services.

APPENDIX

TABLE 5
CANDIDATE MODELS

Model	Ap ^a	NFP ^b	BIC ^c	AIC ^c	SDNR ^c
Channel 1, All Intrapixel Parameters Free:					
1553 points, uncertainties multiplied by 0.30946					
Linear	3.00	11	1622.8	1564.0	0.00232818
Quadratic	3.00	11	1612.1	1553.3	0.00231926
Log+Linear	3.00	12	1624.5	1560.3	0.00232366
Rising Exp	3.00	10	1611.8	1558.3	0.00232512
1544 points, uncertainties multiplied by 0.31028					
Linear	3.25	11	1613.8	1555.0	0.00230984
Quadratic	3.25	11	1602.7	1543.9	0.00230068

TABLE 5 — *Continued*

Model	Ap ^a	NFP ^b	BIC ^c	AIC ^c	SDNR ^c
Log+Linear	3.25	12	1615.1	1551.0	0.00230511
Rising Exp	3.25	10	1602.4	1549.0	0.00230655
1536 points, uncertainties multiplied by 0.31130					
Linear	3.50	11	1605.7	1547.0	0.00229716
Quadratic	3.50	11	1591.8	1533.0	0.00228574
Log+Linear	3.50	12	1605.9	1541.9	0.00229146
Rising Exp	3.50	10	1592.3	1539.0	0.00229226
1532 points, uncertainties multiplied by 0.31286					
Linear	3.75	11	1601.7	1543.0	0.00229111
Quadratic	3.75	11	1588.9	1530.2	0.00228061
Log+Linear	3.75	12	1601.5	1537.5	0.00228509
Rising Exp	3.75	10	1588.8	1535.4	0.00228651
1530 points, uncertainties multiplied by 0.31547					
Linear	4.00	11	1599.7	1541.0	0.00229468
Quadratic	4.00	11	1586.5	1527.8	0.00228382
Log+Linear	4.00	12	1599.2	1535.2	0.00228842
Rising Exp	4.00	10	1586.4	1533.0	0.00228974
Channel 1, Intrapixel with only x^2 and y free:					
1553 points, uncertainties multiplied by 0.30916					
Linear	3.00	8	1603.8	1561.0	0.00232820
Quadratic	3.00	8	1593.0	1550.2	0.00231930
Log+Linear	3.00	9	1605.0	1556.9	0.00232329
Rising Exp	3.00	7	1592.7	1555.3	0.00232514
1544 points, uncertainties multiplied by 0.31013					
Linear	3.25	8	1594.7	1552.0	0.00231106
Quadratic	3.25	8	1583.9	1541.2	0.00230213
Log+Linear	3.25	9	1596.1	1548.1	0.00230627
Rising Exp	3.25	7	1583.4	1546.0	0.00230874
1536 points, uncertainties multiplied by 0.31106					
Linear	3.50	8	1586.7	1544.0	0.00229865
Quadratic	3.50	8	1572.6	1529.9	0.00228619
Log+Linear	3.50	9	1587.0	1539.0	0.00229298
Rising Exp	3.50	7	1573.2	1535.8	0.00229367
1532 points, uncertainties multiplied by 0.31261					
Linear	3.75	8	1582.7	1540.0	0.00229250
Quadratic	3.75	8	1569.7	1527.0	0.00228188
Log+Linear	3.75	9	1583.3	1535.3	0.00228609
Rising Exp	3.75	7	1569.6	1532.3	0.00228781
1530 points, uncertainties multiplied by 0.31521					
Linear	4.00	8	1580.7	1538.0	0.00229595
Quadratic	4.00	8	1567.3	1524.6	0.00228496
Log+Linear	4.00	9	1583.8	1535.8	0.00229263
Rising Exp	4.00	7	1567.2	1529.9	0.00229094
Channel 2, All Intrapixel Parameters Free:					
1465 points, uncertainties multiplied by 0.44456					
No Ramp	3.50	9	1521.6	1474.0	0.00326693
Linear	3.50	10	1501.7	1448.8	0.00323655
Quadratic	3.50	11	1506.8	1448.6	0.00323340
Falling Exp	3.50	11	1509.9	1451.7	0.00323775
1460 points, uncertainties multiplied by 0.44663					
No Ramp	3.75	9	1516.6	1469.0	0.00326495
Linear	3.75	10	1496.9	1444.1	0.00323477
Quadratic	3.75	11	1502.3	1444.1	0.00323189
Falling Exp	3.75	11	1505.1	1446.9	0.00323590
1457 points, uncertainties multiplied by 0.44875					
No Ramp	4.00	9	1513.6	1466.0	0.00326355
Linear	4.00	10	1492.6	1439.7	0.00323181
Quadratic	4.00	11	1497.7	1439.6	0.00322873
Falling Exp	4.00	11	1500.8	1442.7	0.00323302
1449 points, uncertainties multiplied by 0.45211					
No Ramp	4.25	9	1505.5	1458.0	0.00327075
Linear	4.25	10	1483.7	1430.9	0.00323780

TABLE 5 — *Continued*

Model	Ap ^a	NFP ^b	BIC ^c	AIC ^c	SDNR ^c
Quadratic	4.25	11	1488.5	1430.4	0.00323425
Falling Exp	4.25	11	1492.0	1434.0	0.00323913
1435 points, uncertainties multiplied by 0.45715					
No Ramp	4.50	9	1491.4	1444.0	0.00329102
Linear	4.50	10	1470.1	1417.4	0.00325808
Quadratic	4.50	11	1474.8	1416.9	0.00325441
Falling Exp	4.50	11	1478.4	1420.5	0.00325944
Channel 2, Intrapixel With Only y^2 Free:					
1465 points, uncertainties multiplied by 0.44695					
No Ramp	3.50	5	1496.4	1470.0	0.00328991
Linear	3.50	6	1464.4	1432.6	0.00324507
Quadratic	3.50	7	1470.0	1433.0	0.00324266
Falling Exp	3.50	7	1472.6	1435.6	0.00324626
1460 points, uncertainties multiplied by 0.44969					
No Ramp	3.75	5	1491.4	1465.0	0.00329263
Linear	3.75	6	1455.3	1423.6	0.00324297
Quadratic	3.75	7	1461.2	1424.2	0.00324081
Falling Exp	3.75	7	1463.5	1426.5	0.00324417
1457 points, uncertainties multiplied by 0.45194					
No Ramp	4.00	5	1488.4	1462.0	0.00329209
Linear	4.00	6	1450.5	1418.8	0.00324027
Quadratic	4.00	7	1456.2	1419.2	0.00323791
Falling Exp	4.00	7	1458.7	1421.8	0.00324155
1449 points, uncertainties multiplied by 0.45480					
No Ramp	4.25	5	1480.4	1454.0	0.00329562
Linear	4.25	6	1444.5	1412.9	0.00324584
Quadratic	4.25	7	1449.8	1412.9	0.00324293
Falling Exp	4.25	7	1452.9	1415.9	0.00324720
1435 points, uncertainties multiplied by 0.45965					
No Ramp	4.50	5	1466.3	1440.0	0.00331453
Linear	4.50	6	1432.7	1401.1	0.00326654
Quadratic	4.50	7	1437.9	1401.0	0.00326347
Falling Exp	4.50	7	1441.0	1404.1	0.00326791
Channel 3:					
1544 points, uncertainties multiplied by 0.91447					
No Ramp	2.50	2	1556.7	1546.0	0.01066331
Linear	2.50	3	1553.7	1537.6	0.01062468
Falling Exp	2.50	4	1563.2	1541.9	0.01063552
1543 points, uncertainties multiplied by 0.92247					
No Ramp	2.75	2	1555.7	1545.0	0.01063659
Linear	2.75	3	1549.9	1533.9	0.01058879
Falling Exp	2.75	4	1558.7	1537.4	0.01059726
1535 points, uncertainties multiplied by 0.93860					
No Ramp	3.00	2	1547.7	1537.0	0.01080977
Linear	3.00	3	1543.1	1527.1	0.01076529
Falling Exp	3.00	4	1551.7	1530.4	0.01077319
1529 points, uncertainties multiplied by 0.95222					
No Ramp	3.25	2	1541.7	1531.0	0.01103641
Linear	3.25	3	1538.6	1522.6	0.01099631
Falling Exp	3.25	4	1547.6	1526.2	0.01100564
1524 points, uncertainties multiplied by 0.96551					
No Ramp	3.50	2	1536.7	1526.0	0.01132113
Linear	3.50	3	1535.2	1519.2	0.01128630
Falling Exp	3.50	4	1544.0	1522.7	0.01129501
1522 points, uncertainties multiplied by 0.97776					
No Ramp	3.75	2	1534.7	1524.0	0.01163603
Linear	3.75	3	1533.8	1517.8	0.01160264
Falling Exp	3.75	4	1542.3	1521.0	0.01161056
1521 points, uncertainties multiplied by 0.99239					
No Ramp	4.00	2	1533.7	1523.0	0.01201476
Linear	4.00	3	1533.2	1517.2	0.01198222

TABLE 5 — *Continued*

Model	Ap ^a	NFP ^b	BIC ^c	AIC ^c	SDNR ^c
Falling Exp	4.00	4	1541.6	1520.3	0.01198978
Channel 4:					
1467 points, uncertainties multiplied by 0.64001					
No Ramp	2.00	2	1479.6	1469.0	0.01269320
Linear	2.00	3	1470.6	1454.8	0.01262427
Rising Exp	2.00	4	1477.1	1455.9	0.01261620
Log+Linear	2.00	5	1484.4	1458.0	0.01261728
Quadratic	2.00	4	1476.2	1455.0	0.01260762
1467 points, uncertainties multiplied by 0.65283					
No Ramp	2.25	2	1479.6	1469.0	0.01291715
Linear	2.25	3	1466.9	1451.1	0.01283127
Rising Exp	2.25	4	1473.8	1452.6	0.01282649
Log+Linear	2.25	5	1479.7	1453.2	0.01281869
Quadratic	2.25	4	1473.1	1452.0	0.01281909
1464 points, uncertainties multiplied by 0.67232					
No Ramp	2.50	2	1476.6	1466.0	0.01333255
Linear	2.50	3	1467.5	1451.6	0.01326022
Rising Exp	2.50	4	1474.6	1453.4	0.01325764
Log+Linear	2.50	5	1481.6	1455.1	0.01325392
Quadratic	2.50	4	1474.3	1453.1	0.01325268
1455 points, uncertainties multiplied by 0.68250					
No Ramp	2.75	2	1467.6	1457.0	0.01361319
Linear	2.75	3	1459.1	1443.2	0.01354198
Rising Exp	2.75	4	1466.4	1445.2	0.01354054
Log+Linear	2.75	5	1474.2	1447.8	0.01354051
Quadratic	2.75	4	1466.3	1445.2	0.01353948
1448 points, uncertainties multiplied by 0.69698					
No Ramp	3.00	2	1460.6	1450.0	0.01404468
Linear	3.00	3	1451.3	1435.4	0.01396745
Rising Exp	3.00	4	1458.5	1437.4	0.01396580
Log+Linear	3.00	5	1467.0	1440.6	0.01396978
Quadratic	3.00	4	1458.5	1437.3	0.01396422
1443 points, uncertainties multiplied by 0.71158					
No Ramp	3.25	2	1455.5	1445.0	0.01457611
Linear	3.25	3	1443.8	1428.0	0.01448370
Rising Exp	3.25	4	1451.0	1429.9	0.01448177
Log+Linear	3.25	5	1456.9	1430.6	0.01448402
Quadratic	3.25	4	1450.9	1429.8	0.01447941
1440 points, uncertainties multiplied by 0.72888					
No Ramp	3.50	2	1452.5	1442.0	0.01528549
Linear	3.50	3	1437.9	1422.1	0.01517316
Rising Exp	3.50	4	1445.1	1424.0	0.01517067
Log+Linear	3.50	5	1451.3	1424.9	0.01517428
Quadratic	3.50	4	1444.9	1423.8	0.01516664
1431 points, uncertainties multiplied by 0.75781					
No Ramp	4.00	2	1443.5	1433.0	0.01694407
Linear	4.00	3	1424.0	1408.2	0.01679042
Rising Exp	4.00	4	1431.1	1410.1	0.01678704
Log+Linear	4.00	5	1437.9	1411.6	0.01679340
Quadratic	4.00	4	1431.0	1409.9	0.01678180

^a Aperture radius in pixels

^b Number of free parameters (k in the text)

^c Compare between the aperture sizes, for the same model, by SDNR. Compare within the aperture sizes by BIC and AIC.

REFERENCES

- Batygin, K., Bodenheimer, P., & Laughlin, G. 2009, *ApJ*, 704, L49
 Beaulieu, J., Tinetti, G., Kipping, D. M., Ribas, I., Barber, R. J., Y-K. Cho, J., Polichtchouk, I., Tennyson, J., Yurchenko, S. N., Griffith, C. A., Batista, V., Waldmann, I., Miller, S., Carey, S., Mousis, O., Fossey, S. J., & Aylward, A. 2010, *ArXiv*, 1007.0324
 Bodenheimer, P., Laughlin, G., & Lin, D. N. C. 2003, *ApJ*, 592, 555
 Charbonneau, D., Allen, L. E., Megeath, S. T., Torres, G., Alonso, R., Brown, T. M., Gilliland, R. L., Latham, D. W., Mandushev, G., O'Donovan, F. T., & Sozzetti, A. 2005, *ApJ*, 626, 523
 Charbonneau, D., Brown, T. M., Burrows, A., & Laughlin, G. 2007, *Protostars and Planets V*, 701
 Croll, B., Lafreniere, D., Albert, L., Jayawardhana, R., Fortney, J. J., & Murray, N. 2010, *ArXiv*, 1009.0071, *ApJ*, in press
 Eastman, J., Siverd, R., & Gaudi, B. S. 2010, *PASP*, 122, 935

- Fazio, G. G., Hora, J. L., Allen, L. E., Ashby, M. L. N., Barmby, P., Deutsch, L. K., Huang, J., Kleiner, S., Marengo, M., Megeath, S. T., Melnick, G. J., Pahre, M. A., Patten, B. M., Polizotti, J., Smith, H. A., Taylor, R. S., Wang, Z., Willner, S. P., Hoffmann, W. F., Pipher, J. L., Forrest, W. J., McMurty, C. W., McCreight, C. R., McKelvey, M. E., McMurray, R. E., Koch, D. G., Moseley, S. H., Arendt, R. G., Mentzell, J. E., Marx, C. T., Losch, P., Mayman, P., Eichhorn, W., Krebs, D., Jhabvala, M., Gezari, D. Y., Fixsen, D. J., Flores, J., Shakoorzadeh, K., Jungo, R., Hakun, C., Workman, L., Karpati, G., Kichak, R., Whitley, R., Mann, S., Tollestrup, E. V., Eisenhardt, P., Stern, D., Gorjian, V., Bhattacharya, B., Carey, S., Nelson, B. O., Glaccum, W. J., Lacy, M., Lowrance, P. J., Laine, S., Reach, W. T., Stauffer, J. A., Surace, J. A., Wilson, G., Wright, E. L., Hoffman, A., Domingo, G., & Cohen, M. 2004, *ApJS*, 154, 10
- Fortney, J. J., Marley, M. S., & Barnes, J. W. 2007, *ApJ*, 659, 1661
- Gelman, A. & Rubin, D. B. 1992, *Stat. Sci.*, 7, 457
- Giménez, A. & Bastero, M. 1995, *Ap&SS*, 226, 99
- Goldreich, P. & Soter, S. 1966, *Icarus*, 5, 375
- Harrington, J., Luszcz, S., Seager, S., Deming, D., & Richardson, L. J. 2007, *Nature*, 447, 691
- Hebb, L., Collier-Cameron, A., Loeillet, B., Pollacco, D., Hébrard, G., Street, R. A., Bouchy, F., Stempels, H. C., Moutou, C., Simpson, E., Udry, S., Joshi, Y. C., West, R. G., Skillen, I., Wilson, D. M., McDonald, I., Gibson, N. P., Aigrain, S., Anderson, D. R., Benn, C. R., Christian, D. J., Enoch, B., Haswell, C. A., Hellier, C., Horne, K., Irwin, J., Lister, T. A., Maxted, P., Mayor, M., Norton, A. J., Parley, N., Pont, F., Queloz, D., Smalley, B., & Wheatley, P. J. 2009, *ApJ*, 693, 1920
- Husnoo, N., Pont, F., Hébrard, G., Simpson, E., Mazeh, T., Bouchy, F., Moutou, C., Arnold, L., Boisse, I., Diaz, R., Eggenberger, A., & Shporer, A. 2010, *ArXiv*, 1004.1809
- Jackson, B., Greenberg, R., & Barnes, R. 2008, *ApJ*, 678, 1396
- Kallrath, J. & Milone, E. F. 1999, *Eclipsing Binary Stars: Modeling and Analysis* (New York: Springer)
- Knutson, H. A., Charbonneau, D., Allen, L. E., Burrows, A., & Megeath, S. T. 2008, *ApJ*, 673, 526
- Knutson, H. A., Charbonneau, D., Allen, L. E., Fortney, J. J., Agol, E., Cowan, N. B., Showman, A. P., Cooper, C. S., & Megeath, S. T. 2007, *Nature*, 447, 183
- Knutson, H. A., Charbonneau, D., Cowan, N. B., Fortney, J. J., Showman, A. P., Agol, E., & Henry, G. W. 2009, *ApJ*, 703, 769
- Kreiner, J. M., Kim, C., & Nha, I. 2001, *An Atlas of O-C Diagrams of Eclipsing Binary Stars* (Cracow, Poland: Wydawnictwo Naukowe Akademii Pedagogicznej)
- Levrard, B., Winisdoerffer, C., & Chabrier, G. 2009, *ApJ*, 692, L9
- Li, S., Miller, N., Lin, D. N. C., & Fortney, J. J. 2010, *Nature*, 463, 1054
- Little, A. R. 2007, *MNRAS*, 377, L74
- López-Morales, M., Coughlin, J. L., Sing, D. K., Burrows, A., Apai, D., Rogers, J. C., & Spiegel, D. S. 2009, *ArXiv*, 0912.2359
- López-Morales, M., Coughlin, J. L., Sing, D. K., Burrows, A., Apai, D., Rogers, J. C., Spiegel, D. S., & Adams, E. R. 2010, *ApJ*, 716, L36
- MacKay, D. J. C. 2003, *Information Theory, Inference and Learning Algorithms* (New York: Cambridge University Press)
- Madhusudhan, N., Harrington, J., Stevenson, K. B., Nymeyer, S., Campo, C., Wheatley, P. J., Deming, D., Blecic, J., Hardy, R., Lust, N. B., Anderson, D. R., Collier Cameron, A., Britt, C. B. T., Bowman, W. C., Hebb, L., Hellier, C., Maxted, P. F. L., Pollacco, D., & West, R. G. 2010, *Nature*, in press
- Mandel, K. & Agol, E. 2002, *ApJ*, 580, L171
- Mardling, R. A. 2007, *MNRAS*, 382, 1768
- . 2010, *ArXiv*, 1001.4079
- Poddany, S., Brát, L., & Pejcha, O. 2010, *New Astronomy*, 15, 297
- Pont, F., Zucker, S., & Queloz, D. 2006, *MNRAS*, 373, 231
- Ragozzine, D. & Wolf, A. S. 2009, *ApJ*, 698, 1778
- Reach, W. T., Megeath, S. T., Cohen, M., Hora, J., Carey, S., Surace, J., Willner, S. P., Barmby, P., Wilson, G., Glaccum, W., Lowrance, P., Marengo, M., & Fazio, G. G. 2005, *PASP*, 117, 978
- Sivia, D. & Skilling, J. 2006, *Data Analysis: A Bayesian Tutorial*, 2nd edn. (Oxford Univ. Press, USA)
- Stevenson, K. B., Harrington, J., Nymeyer, S., Madhusudhan, N., Seager, S., Bowman, W. C., Hardy, R. A., Deming, D., Rauscher, E., & Lust, N. B. 2010, *Nature*, 464, 1161
- Werner, M. W., Roellig, T. L., Low, F. J., Rieke, G. H., Rieke, M., Hoffmann, W. F., Young, E., Houck, J. R., Brandl, B., Fazio, G. G., Hora, J. L., Gehrz, R. D., Helou, G., Soifer, B. T., Stauffer, J., Keene, J., Eisenhardt, P., Gallagher, D., Gautier, T. N., Irace, W., Lawrence, C. R., Simmons, L., Van Cleve, J. E., Jura, M., Wright, E. L., & Cruikshank, D. P. 2004, *ApJS*, 154, 1
- Winn, J. N. 2009, in *IAU Symposium 253: Transiting Planets*, 99–109
- Winn, J. N., Holman, M. J., Torres, G., McCullough, P., Johns-Krull, C., Latham, D. W., Shporer, A., Mazeh, T., Garcia-Melendo, E., Foote, C., Esquerdo, G., & Everett, M. 2008, *ApJ*, 683, 1076